On the Performance of a New Wireless Communication Compact Multichannel Underwater Receiver Using a Sphere Vector Sensor

Rami Rashid, Erjian Zhang, and Ali Abdi, *Fellow*, *IEEE*

***Abstract*—In this paper, experimental results are presented on the performance of a new underwater communication compact multichannel receiver that utilizes a sphere vector sensor. It measures the *x*, *y* and *z* underwater particle velocity field components, and utilizes them for symbol recovery. Comparison of the sphere vector sensor experimental data with those collected using a scalar sensor receiver suggests that the multichannel nature of the sphere vector sensor receiver can provide a performance improvement for underwater communication. As another result, statistical analysis of the measured underwater particle velocity channels suggests the Student-*t* distribution as a suitable distribution to characterize such channels. This is useful in studies where a statistical model for the particle velocity channels is needed.**

***Index Terms*—Underwater Communication, Vector Sensor, Particle Velocity, Multichannel Receiver.**

I. Introduction

An underwater vector sensor is a multi-signal sensor that measures the vector components of the acoustic field, i.e., the *x*, *y* and *z* components of the acoustic particle velocity. It is widely used in various applications ranging from underwater localization and angle of arrival estimation [1]-[3], to underwater communication [4]-[6]. In contrast, an underwater scalar sensor is a single-signal sensor that measures the scalar component of the acoustic field, i.e., the acoustic pressure. While the underwater acoustic pressure communication channel is extensively studied, underwater acoustic particle velocity communication channels are less investigated. Here we present experimental results on the performance of a new underwater communication compact multichannel receiver using a sphere vector sensor. The vector sensor measures the three underwater particle velocity channels.

The work is supported in part by the National Science Foundation (NSF), Grant IIP-1500123.

The authors are with the Department of Electrical and Computer Engineering, New Jersey Institute of Technology, Newark, NJ 07102 USA (e-mails: raa62@njit.edu, ez7@ njit.edu, ali.abdi@njit.edu).

The existing multichannel underwater communication receivers use arrays of multiple spatially-separated scalar sensors (hydrophones). For example, a twelve-element hydrophone array of length 1.65 m is used in [7]. In general, array size can be an important concern in modern applications of small autonomous underwater vehicles (AUVs) and other small platforms. For example, the 3 kHz medium frequency receive array of a modem [8] designed for the 21-inch diameter Bluefin AUV consists of four hydrophones and is 1.5 m long. Quoted from [8]: "Ideally a longer array would be used, but this is the largest that can be easily installed in the vehicle." Even at higher frequencies, the length of the array is an issue and it is necessary to reduce its size, if it is supposed to fit into the smaller 12.75-inch AUVs [8]. The proposed sphere vector sensor receiver, on the other hand, can serve as a compact-size multichannel alternative and therefore is suitable for practical applications where small underwater platforms and equipment are needed. As explained later in the paper, this is because it measures the three vector components of the acoustic field.

Multichannel reception and processing of communication signals using arrays of scalar sensors - hydrophones - are widely studied in the literature (see [7] as an example). To the best of our knowledge, however, performance of a sphere vector sensor as a single compact multichannel communication receiver is not previously studied. The papers that utilize a vector sensor as an underwater communication receiver, e.g., [4], [5], [6], [9], [10], use a mathematical model of a vector sensor and the signals that it provides. In this paper, however, we consider a segmented sphere that measures the *x*, *y* and *z* acoustic particle velocity signals, and conduct underwater experiments to collect data for performance analysis and modeling. Here are the new contributions of this paper

- Introducing and utilizing a custom-made sphere vector sensor (Fig. 1, 2) as a new communication receiver (as far as we know, an off-the-shelf sphere vector sensor is not available to buy),
- Conducting underwater experiments and collecting data in two different environments, combined with mathematical analysis, to compare the performance of the sphere vector sensor receiver with a conventional scalar sensor receiver,
- Presenting an experimentally-verified statistical distribution model, the Student-*t* distribution, for the *x*, *y* and *z*

acoustic particle velocity channel impulse responses.
To the best of our knowledge, the above studies and results are not previously presented in the open literature.

The rest of the paper is organized as follows. Section II presents definitions of the underwater particle velocity channels and equations for the vector sensor receiver performance analysis. Section III reports the experimental setup, the custom-made vector sensor and how it works, methods used to conduct the underwater experiments in two different environments, the experimental results on the system performance and the statistical distribution of the particle velocity channels. Finally, Section IV presents some concluding remarks.

II. Definitions of the Particle Velocity Channels and the Vector Sensor Receiver

Let $s(t)$ be the transmitted signal. The measured signal $r_p(t)$ that an underwater scalar sensor provides can be written as

$$r_p(t) = h_p(t) \oplus s(t) + n_p(t), \quad (1)$$

where $h_p(t)$ is the underwater acoustic pressure channel impulse response, $\oplus$ represents the convolution, and $n_p(t)$ is the underwater acoustic pressure noise. On the other hand, the measured signals $\mathbf{r}_{x,y,z}(t) = [r_x(t)\ r_y(t)\ r_z(t)]^T$ that an underwater acoustic vector sensor provides along the *x*, *y* and *z* axes, with ^{T} being the transpose, are related to $s(t)$ as follows

$$\mathbf{r}_{x,y,z}(t) = \mathbf{h}_{x,y,z}(t) \oplus s(t) + \mathbf{n}_{x,y,z}(t), \quad (2)$$

where $\mathbf{h}_{x,y,z}(t) = [h_x(t)\ h_y(t)\ h_z(t)]^T$ represents the three underwater acoustic particle velocity channel impulse responses, and $\mathbf{n}_{x,y,z}(t) = [n_x(t)\ n_y(t)\ n_z(t)]^T$ represents the three underwater acoustic particle velocity noises. Since the acoustic particle velocity in a specific direction is the spatial gradient of the acoustic pressure in that direction [11], we have

$$r_i = \partial r_p / \partial i,\ \ h_i = \partial h_p / \partial i,\ \ n_i = \partial n_p / \partial i,\ \ i = x, y, z. \quad (3)$$

Upon transmitting *K* symbols $\mathbf{S} = [s_0 \ldots s_{K-1}]^T$, the measured data that an acoustic vector sensor provides can be written as

$$\mathbf{R}_v = \mathbf{H}_v \mathbf{S} + \mathbf{N}_v,$$
$$\mathbf{R}_v = [\mathbf{R}_x^T \mathbf{R}_y^T \mathbf{R}_z^T]^T,\ \mathbf{H}_v = [\mathbf{H}_x^T \mathbf{H}_y^T \mathbf{H}_z^T]^T,\ \mathbf{N}_v = [\mathbf{N}_x^T \mathbf{N}_y^T \mathbf{N}_z^T]^T. \quad (4)$$

In the above equation, $\mathbf{R}_i = [r_i(0) \ldots r_i(K+M-2)]^T$ and $\mathbf{N}_i = [n_i(0) \ldots n_i(K+M-2)]^T$, $i = x, y, z$, are the i $(K+M-1)\times 1$ received signal and noise vectors, respectively, where *M* is the number of channel taps. Moreover, the i $(K+M-1)\times K$ banded particle velocity channel matrix is given by

$$\mathbf{H}_i = \begin{bmatrix} h_i(0) & & \\ \vdots & \ddots & h_i(0) \\ h_i(M-1) & \ddots & \vdots \\ & & h_i(M-1) \end{bmatrix}, \quad i = x, y, z. \quad (5)$$

The measured data that a scalar sensor provides can be similarly written as $\mathbf{R}_p = \mathbf{H}_p \mathbf{S} + \mathbf{N}_p$, where $\mathbf{R}_p = [r_p(0) \ldots r_p(K+M-2)]^T$, $\mathbf{N}_p = [n_p(0) \ldots n_p(K+M-2)]^T$ and similar to (5), $\mathbf{H}_p$ is the $(K+M-1)\times K$ banded acoustic pressure channel matrix where the non-zero elements of its first column are given by $[h_p(0) \ldots h_p(M-1)]^T$.

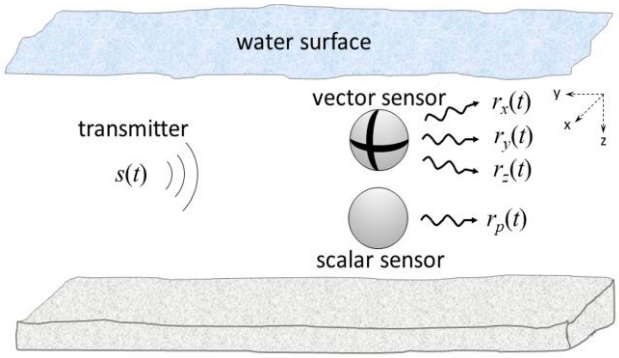

Fig. 1. The proposed multichannel vector sensor communication receiver that utilizes a sphere with eight segments. It provides three signals to be used for symbol recovery, whereas a scalar sensor provides one signal.

For performance comparison and analysis of the proposed vector sensor communication receiver, we consider the minimum variance unbiased estimate of **S** given by [12]

$$\hat{\mathbf{S}}_v = (\mathbf{H}_v^\dagger \boldsymbol{\Sigma}_v^{-1} \mathbf{H}_v)^{-1} \mathbf{H}_v^\dagger \boldsymbol{\Sigma}_v^{-1} \mathbf{R}_v, \quad (6)$$

where † is the transpose conjugate, $\boldsymbol{\Sigma}_v = E[\mathbf{N}_v \mathbf{N}_v^\dagger]$ is the covariance matrix of the particle velocity noise term $\mathbf{N}_v$ in (4), and *E* is the mathematical expectation. In addition to the zero forcing equalizer in (6), other types of equalizers can be used for performance analysis and comparison. Performance of the symbol estimator in (6) is given by the following covariance matrix for the symbol estimation error vector $\hat{\mathbf{S}}_v - \mathbf{S}$ [12]

$$\mathbf{W}_v = E[(\hat{\mathbf{S}}_v - \mathbf{S})(\hat{\mathbf{S}}_v - \mathbf{S})^\dagger] = (\mathbf{H}_v^\dagger \boldsymbol{\Sigma}_v^{-1} \mathbf{H}_v)^{-1}. \quad (7)$$

As a benchmark scalar sensor communication receiver, the corresponding performance analysis equations are

$$\hat{\mathbf{S}}_p = (\mathbf{H}_p^\dagger \boldsymbol{\Sigma}_p^{-1} \mathbf{H}_p)^{-1} \mathbf{H}_p^\dagger \boldsymbol{\Sigma}_p^{-1} \mathbf{R}_p,\ \mathbf{W}_p = (\mathbf{H}_p^\dagger \boldsymbol{\Sigma}_p^{-1} \mathbf{H}_p)^{-1}. \quad (8)$$

Using the estimated **H** and $\boldsymbol{\Sigma}$ matrices from measured data, performance of the two vector and scalar sensor communication receivers are determined and compared in the next section.

III. Empirical Results on the Vector Sensor Receiver Performance and the Particle Velocity Channels

A. The Experimental Setup

For this study and as a compact multichannel communication receiver, we considered a sphere vector sensor [13]. As shown in Fig. 1, it has eight segments on a sphere, and acts as three orthogonal dipoles, similarly to those shown in figure 1 of [14], in the three-dimensional space. Note that each dipole measures one particle velocity component of the field in the corresponding *x*, *y* or *z* direction. More specifically, our custom-made compact multichannel vector sensor (Fig. 2a) is a piezoelectric sphere with eight segments (Fig. 2b). It essentially acts as three orthogonal dipoles - a vector receiver - where each dipole measures the acoustic particle velocity in the corresponding *x*, *y* or *z* direction. By combining the signals of these eight segments appropriately, one can obtain the *x*, *y* and *z* components. For example, the front hemisphere in Fig. 2b,

composed of the segments 1, 2, 5 and 6, acts as one pole of a dipole along the *x* axis. The back hemisphere in Fig. 2b, composed of the segments 3, 4, 7 and 8, serves as the other pole of the dipole along the *x* axis. The overall signals of the front and back hemispheres are $p_1 + p_2 + p_5 + p_6$ and $p_3 + p_4 + p_7 + p_8$, respectively. By computing the signal difference of these two poles, the *x* component can be obtained

$$\begin{aligned} x \text{ component} &= p_3 + p_4 + p_7 + p_8 - (p_1 + p_2 + p_5 + p_6), \\ y \text{ component} &= p_1 + p_4 + p_5 + p_8 - (p_2 + p_3 + p_6 + p_7), \\ z \text{ component} &= p_1 + p_2 + p_3 + p_4 - (p_5 + p_6 + p_7 + p_8). \end{aligned} \quad (9)$$

The *y* component in (9) is extracted by computing the difference between the overall signals of the left and right hemispheres, given by $p_1 + p_4 + p_5 + p_8$ and $p_2 + p_3 + p_6 + p_7$, respectively. Additionally, the *z* component in (9) is obtained by calculating the difference between the overall signals of the top and bottom hemispheres, given by $p_1 + p_2 + p_3 + p_4$ and $p_5 + p_6 + p_7 + p_8$, respectively.

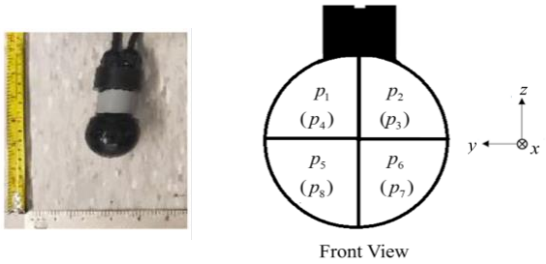

a **b**

Fig. 2. The underwater sphere vector sensor: (a) A picture of our custom-made sphere vector sensor, (b) A schematic diagram of the sensor with eight segments, where the $p_1, p_2, p_5,$ and p_6 segments are on the front hemisphere and the p_3, p_4, p_7 and p_8 segments are on the back hemisphere. The *x* axis is perpendicular to the *y* and *z* axes and points inward, away from the viewer.

The experiments were conducted using the sphere vector sensor of Fig. 2 connected to an analog-to-digital converter, to collect the transmitted signals and bring them into a laptop for further processing and analysis. The experiments were conducted in two different environments and resulted in the following two different datasets. The used methods for collecting these datasets are explained in the next subsection.

Dataset 1: The first dataset was obtained by transmitting one hundred chirp signals in a large pool. The duration and bandwidth of each chirp were 200 msec and 8 kHz, centered at 20 kHz, and the spacing between each two consecutive chirps was 200 msec. The complex baseband chirp signal is given by

$$s_{\text{chirp}}(t) = \exp(j2\pi B_0 (2T_0)^{-1} t^2), \quad (10)$$

where $j^2 = -1$, B_0 is the signal bandwidth and T_0 is the signal duration. Experiments were performed along the pool length, whose size was nearly 23×13 m, and its depth varied from approximately 1 to 3 m. The transmitter and receiver were about 20 m far apart, and were about 0.6 m below the water surface. There were some swimming activities in some other lanes during the measurements.

Dataset 2: The second dataset was collected by transmitting fifty blocks of pilot symbols in shallow waters off Woods Hole, MA, where the pilot symbols were quadrature phase shift keying (QPSK) symbols placed at equally-spaced frequencies called pilot tones. The duration and bandwidth of each block were 256 msec and 4 kHz, centered at 20.4 kHz, and the spacing between each two successive blocks was 25 msec. The distance between the transmitter and receiver was 26 m, about the same as the dataset 1 distance, to have a fair comparison. The transmitter and receiver were 15 m below the water surface.

B. The Channel Estimation Methods

To estimate the particle velocity channel matrix $\mathbf{H}_v = [\mathbf{H}_x^T \quad \mathbf{H}_y^T \quad \mathbf{H}_z^T]^T$ to substitute in (7) for performance analysis, the chirp-based and the pilot-based methods were used to estimate the channel impulse responses.

Chirp-based method: This method was used in the experiments conducted to collect dataset 1. The essence of this method for channel estimation is as follows. Upon transmitting $s_{\text{chirp}}(t)$ that is given in (10), it is convolved with the unknown channel impulse response $h(t)$. If this received signal $h(t) \oplus s_{\text{chirp}}(t)$ is passed through a filter whose impulse response is matched to the chirp signal, that is, $h_{\text{MF}}(t) = s_{\text{chirp}}^*(-t)$, with * being the complex conjugate, then at the output of the matched filter we have $\xi_{\text{MF}}(t) = (h(t) \oplus s_{\text{chirp}}(t)) \oplus h_{\text{MF}}(t) = h(t) \oplus (s_{\text{chirp}}(t) \oplus s_{\text{chirp}}^*(-t))$. The last convolution is the autocorrelation function of $s_{\text{chirp}}(t)$ [15] that approaches the delta function when $B_0 T_0 >> 1$, which results in $\xi_{\text{MF}}(t) = h(t)$. This means the output of the matched filter provides us with the measured channel impulse response. In our experiments we had $B_0 T_0 = 1600 >> 1$.

Pilot-based method: This method was utilized in the performed experiments to collect dataset 2. In this method and at the transmitter side, pilot phase shift keying (PSK) symbols are placed at equally-spaced frequencies called pilot tones. The pilot symbols and their corresponding frequencies are known to both of the transmitter and receiver. Upon performing inverse fast Fourier transform, a time-domain waveform is generated and then transmitted. By performing fast Fourier transform at the receiver side, followed by extracting the received data at the pilot tones and then plugging them into a closed-from least squares estimation formula [16], the measured channel impulse response is obtained.

To estimate the particle velocity noise covariance matrix $\mathbf{\Sigma}_v$ to substitute in (7) for performance analysis, we used the waveforms recorded for several seconds, when there was no signal transmission. Examining the auto- and cross-covariance sequences for the measured *x*, *y* and *z* noise particle velocity components suggested $\mathbf{\Sigma}_v = \text{diag}(\sigma_x^2, \sigma_y^2, \sigma_z^2) \otimes \mathbf{I}_{K+M-1}$, where diag represents a diagonal matrix, $\sigma_i^2 = E[|n_i(t)|^2]$, $i = x, y, z,$

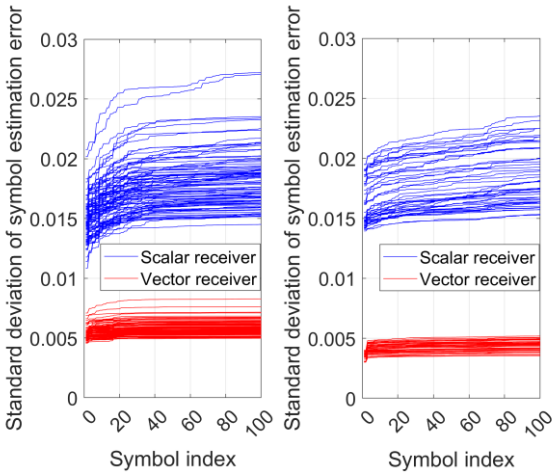

Fig. 3. Sorted square roots of the diagonal elements of the symbol estimation error covariance matrices $\mathbf{W}_v$ and $\mathbf{W}_p$ for the vector and scalar receivers in red and blue, respectively: (a) Dataset 1, (b) Dataset 2.

is the average power of the i component of the noise particle velocity, $\otimes$ is the Kronecker product and $\mathbf{I}_{K+M-1}$ is the identity matrix of size $K+M-1$. The term diag indicates uncorrelated particle velocity noise components (maybe attributed to a possibly noise field isotropic distribution [6]). To perform a hypothesis testing statistical analysis to verify our observations, we used the Ljung-Box (LB) test [17]. In both datasets, the LB test did not reject the null hypothesis that the noise components were uncorrelated, at the 5% significance level.

C. Experimental Results on the Symbol Estimation Errors

By substituting the measured $\mathbf{H}_v$ and $\mathbf{\Sigma}_v$ channel and noise matrices in (7), sorted square roots of the diagonal elements of the symbol estimation error covariance matrix $\mathbf{W}_v$ are computed and plotted in Fig. 3 for both datasets, for the vector sensor receiver. By adding up all the segments of the same sphere, one can have a scalar sensor receiver, whose equations and performance are given in (8). The acoustic pressure channel matrix $\mathbf{H}_p$ was similarly estimated multiple times in both datasets and using the same methods, all explained in Section III. Sorted square roots of the diagonal elements of $\mathbf{W}_p$ are plotted in Fig. 3 for both datasets, for the scalar sensor receiver.

Fig. 3 shows that in both datasets, the vector receiver offers smaller symbol estimation errors, compared to the scalar receiver. This can be attributed to the matter that the vector receiver utilizes multiple channels for symbol detection. Additionally, the vector receiver offers signal-to-noise ratio (SNR) advantage. More specifically, average SNRs in dB ± the standard deviations in dataset 1 for the x, y, z and p channels are 22.9 ± 0.9, 22.5 ± 0.7, 13.7 ± 0.7, and 17.7 ± 0.9, respectively. Additionally, in dataset 2 and for the x, y, z and p channels we have 29.9 ± 1, 29.7 ± 0.5, 18.2 ± 0.6, and 18.9 ± 0.9, respectively. The lower values for the z channel may be attributed to more signal attenuation due to more reflections.

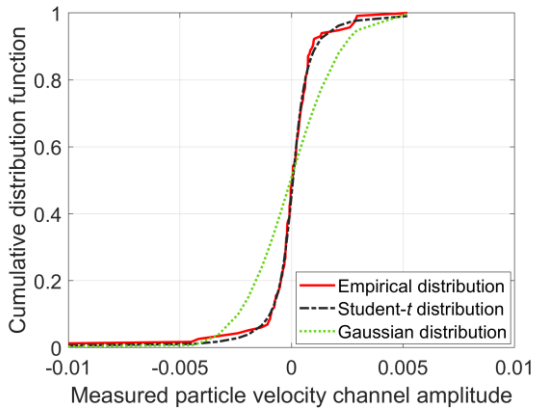

Fig. 4. A representative example of the empirical distribution of a measured underwater acoustic particle velocity channel impulse response amplitude, together with the Student-t distribution and the Gaussian distribution.

Each SNR is calculated as the average signal power divided by the average noise power, where the average power of a $U\times 1$ complex vector $\mathbf{u}$ is given by $U^{-1}\mathbf{u}^{\dagger}\mathbf{u}$.

D. Statistical Distribution of the Particle Velocity Channels

When it comes to analytical studies in the underwater acoustic pressure channel, Gaussian distribution is typically used for its mathematical convenience [18]-[19]. Therefore, to find a distribution for the underwater acoustic particle velocity channels, we started with the Gaussian distribution. As a representative example, empirical cumulative distribution function (CDF) of the real part of the x particle velocity channel impulse response h_x for dataset 1 is shown in Fig. 4, together with a Gaussian CDF whose parameters are estimated using the maximum likelihood (ML) method. We observed that the Gaussian CDF does not exhibit a close fit to the data. We verified this using the Pearson chi-square goodness-of-fit statistical hypothesis test [20], that rejected the null hypothesis of the data being distributed according to the Gaussian model, at the 5% significance level. Additionally, this null hypothesis was rejected for the real and imaginary parts of h_x, h_y and h_z for both datasets.

Contrary to the Gaussian distribution, our further statistical analysis of the collected data revealed that the Student-t distribution served as a more accurate model. The Student-t distribution is more general than the Gaussian distribution and includes it as a special case. Moreover, and as an elliptically symmetric distribution, the Student-t distribution enjoys many useful properties of the Gaussian distribution [21]. These make the Student-t distribution suitable for analytical studies, e.g., [18]-[19], when conducted for the underwater acoustic particle velocity channels. The Student-t probability density function (PDF) is given by $f(\zeta)=\Gamma((\kappa+1)/2)(\eta\sqrt{\pi\kappa}\Gamma(\kappa/2))^{-1}(1+\kappa^{-1}\eta^{-2}(\zeta-\mu)^2)^{-(\kappa+1)/2}$, where $\Gamma(.)$ is the gamma function and μ, η and κ are the

location, scale and shape parameters, respectively. When $\kappa \to \infty$, it approaches a Gaussian PDF with the mean μ and standard deviation η.

As a visual example and for the same particle velocity channel impulse response data shown in Fig. 4, a Student-*t* CDF whose parameters are estimated using the ML method is also graphed. Contrary to the Gaussian CDF, the Student-*t* CDF shows a very close fit to the data. We confirmed this observation using the Pearson chi-square goodness-of-fit statistical hypothesis test [20], that did not reject the null hypothesis of the data being distributed according to the Student-*t* distribution, at the 5% significance level. Furthermore, the Student-*t* null hypothesis was not rejected for any of the real and imaginary parts of h_x, h_y and h_z in both datasets. This is while as mentioned previously, the Gaussian distribution null hypothesis was rejected for both datasets, for all of the real and imaginary parts of h_x, h_y and h_z.

IV. Conclusion

The propagation field in an underwater environment exhibits vector and scalar components. Acoustic particle velocity is the three-dimensional vector component, whereas acoustic pressure is the scalar component. In this paper and using experimental data, performance of the three *x*, *y* and *z* particle velocity communication channels and the acoustic pressure communication channel are compared. The particle velocity channels are measured using a new sphere vector sensor receiver. It appears that the vector sensor receiver offers smaller symbol estimation errors. This can be because of the multi-signal nature of the vector sensor receiver that utilizes multiple channels for symbol recovery. The compact size of this multichannel sensor is another advantage that makes it suitable for small underwater equipment and platforms. Another result learned from analyzing the measured data is that the underwater particle velocity channels can be modeled using the Student-*t* distribution. This is helpful in research studies that require a statistical channel model distribution.

References

[1] A. Nehorai and E. Paldi, "Acoustic vector-sensor array processing," *IEEE Trans. Signal Processing*, vol. 42, pp. 2481-2491, 1994.

[2] X. Zhong, A. B. Premkumar, and H. Wang, "Multiple wideband acoustic source tracking in 3-D space using a distributed acoustic vector sensor array," *IEEE Sensors J.*, vol. 14, pp. 2502-2513, 2014.

[3] X. Zhong and A. B. Premkumar, "Particle filtering approaches for multiple acoustic source detection and 2-D direction of arrival estimation using a single acoustic vector sensor," *IEEE Trans. Signal Processing*, vol. 60, pp. 4719- 4733, 2012.

[4] M. Rawat, B. Lall, and S. Srirangarajan, "Statistical modeling and performance analysis of cooperative communication in frequency-selective underwater acoustic channel using vector sensor," *IEEE Sensors J.*, vol. 21, pp. 7367-7379, 2021.

[5] F. Fauziya, B. Lall, and M. Agrawal, "Impact of vector sensor on underwater acoustic communications system," *IET Radar, Sonar Navigation*, vol. 12, pp. 1500-1508, 2018.

[6] A. Abdi and H. Guo, "A new compact multichannel receiver for underwater wireless communication networks," *IEEE Trans. Wireless Commun.*, vol. 8, pp. 3326-3329, 2009.

[7] M. Stojanovic and L. Freitag, "Multichannel detection for wideband underwater acoustic CDMA communications," *IEEE J. Oceanic Eng.*, vol. 31, pp. 685 - 695, 2006.

[8] L. E. Freitag, M. Grund, J. Partan, K. Ball, S. Singh, and P. Koski, "Multi-band acoustic modem for the communications and navigation aid AUV," in *Proc. Oceans*, Washington, DC, 2005, pp. 1-6.

[9] K. Wang, J. He, T. Shu, and Z. Liu, "Joint angle and delay estimation for underwater acoustic multicarrier CDMA systems using a vector sensor," *IET Radar Sonar Navig.*, vol. 10, pp. 774-783, 2016.

[10] J. He, M. N. S. Swamy, and M. O. Ahmad, "Joint space-time parameter estimation for underwater communication channels with velocity vector sensor arrays," *IEEE Trans. Wireless Commun.*, vol. 11, pp. 3869-3877, 2012.

[11] A. D. Pierce, *Acoustics: An Introduction to Its Physical Principles and Applications*, 2nd ed., Acoustic Soc. Am., 1989.

[12] S. M. Kay, *Fundamentals of Statistical Signal Processing: Estimation Theory*, PTR Prentice-Hall, 1993.

[13] H. Saheban and Z. Kordrostami, "Hydrophones, fundamental features, design considerations, and various structures: A review," *Sensors and Actuators, A: Physical*, vol. 329, 112790, 2021.

[14] A. Abdi, H. Guo, A. Song, and M. Badiey, "An overview of underwater acoustic communication via particle velocity channels: Channel modeling and transceiver design," in *Proc. Meetings on Acoustics*, vol. 9, 2010, pp. 1-5.

[15] A. Springer, M. Huemer, L. Reindl, C. C. W. Ruppel, A. Pohl, F. Seifert, W. Gugler, and R. Weige, "A robust ultra-broad-band wireless communication system using saw chirped delay lines," *IEEE Trans. Microw. Theory Tech.*, vol. 46, pp. 2213-2219, 1998.

[16] B. Li, S. Zhou, M. Stojanovic, and L. Freitag, "Pilot-tone based ZP-OFDM demodulation for an underwater acoustic channel," in *Proc. Oceans*, Boston, MA, 2006, pp. 1-5.

[17] G. E. P. Box, G. M. Jenkins, G. C. Reinsel, and G. M. Ljung., *Time Series Analysis: Forecasting and Control*, 5th ed., Wiley, 2016.

[18] B. Friedlander and A. Zeira, "Detection of broadband signals in frequency and time dispersive channels," *IEEE Trans. Signal Processing*, vol. 44, pp. 1613-1622, 1996.

[19] R. Rashid, E. Zhang, A. Abdi, and Z.-H. Michalopoulou, "Theoretical and experimental multi-sensor signal detection in time spreading distortion underwater channels," in *Proc. Oceans*, Hampton Roads, VA, 2022, pp. 1-4.

[20] R. V. Hogg, J. W. McKean, and A. T. Craig, *Introduction to Mathematical Statistics*, 8th ed., Pearson, 2019.

[21] N. C. Giri, *Multivariate Statistical Analysis*, 2nd ed., Marcel Dekker, 2004.